Review response version submitted to The Cryosphere Discussions, 06 October 2014;
Contact: T. Scambos, teds@nsidc.edu, 303/492-1113

Detailed ice loss pattern in the northern Antarctic Peninsula: widespread decline driven by ice front retreats

Ted A. Scambos[1], Etienne Berthier[2], Terry Haran[1], Christopher A. Shuman[3], Alison J. Cook[4], Stefan R. M. Ligtenberg[5], and Jennifer Bohlander[1]

[1]National Snow and Ice Data Center (NSIDC), University of Colorado at Boulder, Boulder CO 80303 USA

[2]Laboratoire d'Etudes en Géophysique et Océanographie Spatiales, Centre National de la Recherche Scientifique (LEGOS CNRS), Université de Toulouse, Toulouse 31400 France

[3]University of Maryland, Baltimore County, Joint Center for Earth Technology (UMBC JCET) at NASA Goddard Space Flight Center, Greenbelt, MD 20771 USA

[4]Department of Geography, Swansea University, Swansea SA2 8PP UK

[5]Institute for Marine and Atmospheric Research Utrecht (IMAU), Utrecht 3508 TA Netherlands

Corresponding author: T.A. Scambos (National Snow and Ice Data Center, University of Colorado, Boulder, 1540 30th Street Bldg. RL-2, Boulder CO 80303, teds@nsidc.edu, +1-303-492-1113).

Abstract

The northern Antarctic Peninsula (nAP, <66°S) is one of the most rapidly changing glaciated regions on Earth, yet the spatial patterns of its ice mass loss at the glacier basin scale have to date been poorly documented. We use satellite laser altimetry and satellite stereo-image topography spanning 2001-2010, but primarily 2003-2008, to map ice elevation change and infer mass changes for 33 glacier basins covering the mainland and most large islands in the nAP. Rates of ice volume and ice mass change are 27.7±8.6 km^3 a^{-1} and 24.9±7.8 Gt a^{-1}. Mass loss is highest for eastern glaciers affected by major ice shelf collapses in 1995 and 2002, where twelve glaciers account for 60% of the total imbalance. However, losses at smaller rates occur throughout the nAP, at both high and low elevation, despite increased snow accumulation along the western coast and ridge crest. We interpret the widespread mass loss to be driven by decades of ice front retreats on both sides of the nAP, and extended throughout the ice sheet due to the propagation of kinematic waves triggered at the fronts into the interior.

(184 words)

Index terms:
Ice Shelves; Glaciers; Mass Balance; Remote Sensing; Instruments and techniques

Keywords:
Antarctic Peninsula; ICESat; DEM differencing; Larsen B; Larsen A; Prince Gustav

1 Introduction

The nAP is one of two areas of the Antarctic Ice Sheet showing major mass loss, the other being the Amundsen Sea coast of West Antarctica's ice sheet. Previous studies have shown large negative mass imbalances and significant elevation losses for the nAP (*Ivins et al.*, 2011; *Shepherd et al.*, 2012; *Luthcke et al.*, 2013; *Sasgen et al.*, 2013; *McMillan et al.,* 2014). However, in general these studies have not resolved the spatial distribution of mass imbalance in detail, nor attempted to link patterns of ice loss to processes responsible for the loss. Studies based on gravitational change detection using the Gravity Recovery and Climate Experiment satellite system (GRACE) have an inherent spatial resolution of roughly 250 km scale (*Ivins et al.*,

2011; *Luthcke et al.*, 2013; *Sasgen et al.*, 2013), far larger than the scale of the nAP individual glacier basins and islands. Past altimetry-based studies (*Pritchard et al.*, 2009; *Flament and Rémy*, 2012; *Shepherd et al.*, 2012; *McMillan et al.*, 2014) suffer from either sparse coverage or slope correction issues, or both, due to the steep terrain in the nAP. In the published assessments based on laser altimetry (*Shepherd et al.*, 2012), broad assumptions and large extrapolations are required to interpolate the data across the dissected and rugged Peninsula region. Mass budget methods (*Rignot et al.*, 2004, 2008; *Rott et al.*, 2011; *Shepherd et al.*, 2012), which aim to difference outflowing ice flux and surface mass balance (SMB) for each glacier basin have to date shown results that are difficult to reconcile with other studies of the same glaciers (*Shuman et al.*, 2011; *Berthier et al.*, 2012). This is primarily due to spatially coarse SMB estimates from models or field measurements, difficulties in estimating the cross-sectional area of the glaciers, and differences in the span of time used to estimate ice flux changes (*Berthier et al.*, 2012).

The goal of this study is to determine the spatial pattern of ice elevation changes in the nAP, improve estimates of mass balance for the region, and study the relationship of mass balance with ice shelf collapse and ice front retreats in the area. In light of known climate-related changes in the region, such as increasing surface air temperatures and surface melting, regional sea ice decline, and increasing accumulation (e.g., *Mulvaney et al.* 2012; *Zagorodnov et al.*, 2012; *Stammerjohn et al.,* 2008; *Lenaerts et al.,* 2012; *Barrand et al.*, 2013), our study reveals a pattern of ice mass loss in space and (we infer) in time that may be similar to the characteristics of mass loss in other areas of Antarctica in the coming century.

2 Methods

Our study combines satellite stereo-image digital elevation model differencing (dDEM) with repeat-track laser altimetry from the Ice, Cloud and land Elevation Satellite (ICESat; *Schutz et al.,* 2005), with the objective of providing an assessment of surface elevation change resolved at the scale of the major glacier catchments. We use stereo-image data from the Advanced Spaceborne Thermal Emission and

Reflection Radiometer (ASTER; *Fujisada et al.*, 2005) and Satellite Pour l'Observation de la Terre 5 (SPOT5; *Korona et al.*, 2009). Eight satellite stereo-image data sets from the ASTER sensor, and six from the SPOT-5 Haute Résolution Stéréoscopique (HRS) sensor (Table S1 and Figure S1) were processed using previously published methods (*Shuman et al.*, 2011; *Berthier et al.*, 2012; *Gardelle et al.*, 2013).

For the ICESat repeat-track data (Release 633), we used 26 ground tracks from the 91-day-repeat orbit crossing the nAP and major ice-covered islands for the high-energy laser campaigns (ICESat Laser 2A through Laser 3J, September 2003 – March 2008; *Shuman et al.,* 2006; *Zwally et al.*, 2012). Cross-track elevation adjustment and along-track filtering are used to improve measurement quality, based on surface slopes (not elevations) derived from a recent Antarctic Peninsula DEM (*Cook et al.*, 2012). We first eliminated ICESat profile tracks more than 300 meters from the reference track position, and sections where the absolute slope from the gridded DEM was > ±10% slope (or ±5.7°) for the reference track or measurement track location, or areas where the absolute difference between along-track slopes of the measurement track and reference track exceeded 5% (or ±2.86°). We further required the ICESat elevation data to be within 50 m (vertically) of the corresponding interpolated DEM elevation. All elevations are referenced to the EGM96 geoid datum. To migrate the measurement track data to the reference track and compare elevations, we identified reference track 'stations' every 43.75 m along the reference track (one-fourth the distance between ICESat altimetry shot locations along track). We then applied an elevation correction based on the difference between the interpolated gridded DEM elevation at the nearest reference track station and the ICESat track data point. ICESat campaign data were compared by differencing their migrated elevations, divided by the time in years between dates of track acquisition. To reduce effects of possible seasonal variations in elevation, we compared only near-integer-year separated repeat profiles, e.g., data from campaigns 2A to 3A (~October, ~1 year apart) or 3B to 3H (~March, ~2 years apart).

To evaluate different processes in elevation and ice mass change, we treat regions above and below 1000 m above sea level (a.s.l.) separately for each of 33 drainage basins. This is the approximate elevation of an extensive escarpment in the nAP separating plateau areas from individual glacier cirques. Above 1000 m a.s.l., and for islands without sufficient dDEM coverage (Robertson Is., Snow Hill Is., and Joinville, Dundee, and D'Urville islands; Figure 1), the rate of elevation change (dH/dt) is determined from satellite laser altimetry alone. In smooth high elevation areas, correlation of satellite stereo-images often fails due to a lack of high-contrast surface features of sufficient horizontal scale (tens of meters). Below 1000 m a.s.l., a hypsometric interpolation method was applied to individual glacier basins to extend dDEMs and ICESat dH/dt measurements to areas not directly measured. ICESat dH/dt was weighted 10-fold relative to dDEM dH/dt to prevent small dDEM data areas from dominating the weighted dH/dt mapping, and to better utilize the higher accuracy of individual ICESat-based measurements. We used the relationship

$$dH/dt_{hyps} = (dH/dt_{DEM}*(N_{DEM}/e_{DEM})+dH/dt_{ICESat}*(N_{ICESat}/e_{ICESat}))/((N_{DEM}/e_{DEM})+(N_{ICESat}/e_{ICESat})) \quad (1)$$

where N is the number of measurements within an elevation band (i.e., the number of 50 m grid cells for the dDEMs; or reference track site locations at 43.75 m spacing for ICESat) and e is an inverse weighting of the measurement methods. For dDEMs we used a weight of 1, and for ICESat, we used 0.1. This allowed the fewer but more accurate ICESat-based measurements to contribute to the final result in basins with extensive dDEM coverage. In several areas, ICESat data were available in regions not well covered by dDEM results (see Figure S2).

We also estimate the above-flotation mass loss of grounded-ice areas that retreated at least 2 km^2 during the study interval (2001-2010), as identified by image mapping (*Cook et al.*, 2005; *Cook and Vaughan*, 2010). To estimate the volume and mass loss represented by these areas we mapped the area of retreat during our study period (2001-2010) and half the mean elevation loss rate observed just above

155 the area of grounded ice retreat. This represents an assumption that the vertical
156 elevation change rate of the retreated ice was identical to the region just upstream
157 of the loss area, and that the time of ice front retreat (e.g., when the ice calved and
158 drifted away) was midway through the study period.
159
160 Errors for our assessment of dH/dt (Tables 1 and S2), are based on past analysis of
161 the dDEM method (*Shuman et al.*, 2011; *Berthier et al.*, 2012), on inter-comparisons
162 of the two methods at sites having both dDEM and ICESat measurements, and on
163 crossover analysis of ICESat cross-track-corrected data (Table S4). Past analysis for
164 this region suggests that dDEM methods using mixed ASTER and SPOT5 imagery
165 can have a ±5 m uncertainty for individual glacier basins, i.e. ~1 m a^{-1} given a 5-yr
166 time separation between DEMs. However, examining our ICESat and dDEM dH/dt at
167 sites with both measurements (6158 sites) shows that the methods differ by just
168 ~0.3 m a^{-1} overall, a difference that ranges between 0.07 to 0.75 m a^{-1} over various
169 sub-sets of our measurements (Table S4). This is in agreement with our previous
170 study that showed reduced errors when dDEM results are averaged over basin-scale
171 areas (*Berthier et al.*, 2012). Seven crossover sites with slope-corrected ICESat
172 dH/dt measurements show good agreement with the dDEM measurements at the
173 same locations (mean offset of +0.05 m a^{-1}).
174
175 Errors in the ICESat cross-track correction for dH/dt are more dependent on slope
176 errors in the Cook et al. (2012) DEM and not its absolute elevation accuracy.
177 Assuming our selection criteria eliminated regions of significant error in the DEM,
178 we estimate that across-track or along-track slopes in the Cook et al. (2012) DEM
179 are accurate to within ±0.5° over a length scale of 300 m, or ±8.7 m km^{-1}. A test of
180 this was conducted by comparing the Cook et al. (2012) DEM slopes with a DEM
181 acquired in 2009 by the NASA Land, Vegetation, and Ice Sensor (LVIS) airborne laser
182 altimeter, covering about 20% of the study region. This showed that the mean
183 difference in along-track slope in the overlap region was 0.06 ± 1.2° when our
184 criteria are applied to both data sets. For laser altimetry measurements alone, our
185 inferred mean slope error of ±0.5° implies a mean laser measurement pair cross-

track correction error of ±1.31 m (assuming a mean cross-track distance of 150 m). We assume this error is randomly distributed when averaging over a glacier basin. Thus for the average of 20 measurement sites, the mean error is <25 cm. Since laser measurement pairs may have 1 to 4 years separation in time, and many have multiple measurements at a single site (see Figure S2), our overall mean error in elevation change rate is significantly less than this. Additionally, the majority of the basins we consider have many more than 20 measurement sites (Table S2).

Considering all sources of error, and variations in the time-span of measurements for dDEM and ICESat measurements, data density variations for the basins, and the strong agreement between these independent altimetric methods, we adopt a mean error of ±0.15 m a^{-1} for regions of laser altimetry measurement alone (above 1000 m a.s.l.), and ±0.3 m a^{-1} for our dDEM plus altimetry measurements (below 1000 m a.s.l.) and the glacier basins, islands, and sub-basins without laser altimetry. Errors for volume and mass change determinations thus scale with area.

3 Results

An overview of our results is shown in Figure 2 and Table 1, and detailed basin-by-basin values are provided in supplementary Table S2. The results show that basins impacted by recent ice shelf loss and ice front retreat have very high rates of change, but also indicate that few areas — high or low, east or west — have positive dH/dt. Recent ice-shelf loss (ISL) basins (losses since 1986, and particularly in 1995 and 2002), all on the eastern side of the nAP, and four smaller glaciers with recent grounded ice front loss (IFL; loses since 2000) on the western and northeastern side of the nAP, show a characteristic pattern of very high elevation loss rates just upstream of the ice front but far lower elevation loss rates at high elevation. Mean elevation change for areas below 1000 m a.s.l. at 12 eastern-side ISL glacier basins (or sub-basins) is -2.6 m a^{-1} (range, +0.4 to -5.8 m a^{-1}) and -2.2 m a^{-1} (-2.0 to -2.7 m a^{-1}) for the four western-side and northeastern IFL sub-basins experiencing recent ice front retreat (>2 km^2 since 2000). At elevations >1000 m, elevation loss in the eastern ISL basins is small (mean, -0.10 m a^{-1}; range +0.35 to -0.54 m a^{-1}). Glacier

systems on the western nAP coast and the western islands below 1000 m a.s.l., excluding the recent IFL regions, are changing at various rates (typically ~-0.15 m a^{-1}, range +0.7 to -1.6 m a^{-1}). However, western-side basins are losing elevation at significant rates above 1000 m a.s.l. (mean of -0.59 m a^{-1}; range -0.25 to -1.30 m a^{-1}).

We examine the rates of surface elevation change and cumulative ice volume change as they vary with altitude for three sub-regions of the study area in Figure 3. The patterns of elevation change with altitude illustrate the differences between the western-side glacier and island regions and the eastern-side ISL areas, and also highlight the bi-modal hypsometry pattern characteristic of the nAP. Eastern-side ISL areas show dramatically decreasing elevation with time, large volume changes at low elevations, and little or no significant change in the upper-most catchment areas (Figure 3c-d). Western-side glaciers show mildly negative rates of elevation change at all elevations, and a steady cumulative volume decrease rate with altitude. The major glaciers of Scar Inlet Ice Shelf, the lone remaining large (>50 km^2) ice shelf in the study area with significant tributary glaciers, show a unique pattern of ice losses at low elevation and some areas of thickening at altitude. We believe this is likely the pattern of elevation change present for the eastern nAP ISL glacier systems in the years immediately prior to shelf disintegration.

4 Discussion

The widespread elevation losses suggested here for both sides of the nAP at high elevations, and especially for the western side of the divide, have significant implications for the region's recent mass change history. Moreover, the detailed mapping on a basin-by-basin scale supports model and GPS studies of local bedrock uplift. A recent study (*Neild et al.,* 2014), using an earlier (near-final) version of our presented data combined with continuous GPS uplift measurements at sites in the Peninsula, modelled both the elastic response and long-term isostatic rebound in the region, showing that the nAP is underlain by very low viscosity mantle. They further conclude that there is little or no continuing uplift (observed or modelled) as a result of mass loss during the Last Glacial Maximum (LGM). The results are

supported by the general conclusions of papers discussing the post-LGM evolution of the eastern Peninsula (*Domack et al.,* 2005; *Rebesco et al.,* 2014) which state that the majority of ice sheet retreat occurred by about 12,000 years ago. If so, mantle rebound from those events would be complete at this point.

Previous observational studies have shown that the elevation decline pattern for ISL or IFL glaciers migrates upstream and diffuses on a scale of years to decades (*Howat et al.*, 2007; *Joughin et al.*, 2008; *Shuman et al.*, 2011; *Berthier et al.*, 2012), consistent with kinematic wave models of glacier response to ice front stress changes for tidewater glaciers (*Pfeffer*, 2007; *Nick et al.*, 2009; *Favier et al.*, 2014). In past work in this area (*Shuman et al.*, 2011; *Berthier et al.*, 2012), and with comparison to these results, we observe that eastern ISL glaciers are currently propagating kinematic waves upstream from their lower trunk areas, but this process has not yet had a significant impact on higher elevations. Western-coast nAP glacier front retreats, elevation losses, and accelerations have been documented (*Cook and Vaughan,* 2005; *Pritchard and Vaughan*, 2007; *Kunz et al.*, 2012), with a major pulse of retreat beginning in the 1970s. Moreover, our work here shows that on-going ice front losses within the study period behave much like smaller versions of the eastern-side glaciers impacted by ice shelf and glacier front retreat (Table 1). The earlier losses inferred for the western side fjord glaciers (e.g., *Christ et al*., 2014) appear to have now propagated throughout the entirety of the western basins, leading to significant and widespread surface lowering in the western upper catchment areas (>1000 a.s.l.) at greater rates than for the eastern side on average (Table 1 and Table S2).

However, any measurement of elevation or mass losses along the western coast and in the upper elevation areas must be reconciled with a large recent positive mass accumulation anomaly. Ice cores at two sites on the nAP ridge crest (Detroit Plateau, 64.08°S, 59.65°W, 1937 m a.s.l., and Site Beta of the Larsen Ice Shelf System, Antarctica, 66.03°S, 64.04°W, 1980 m a.s.l.; Figure 1) show significant increases in accumulation in the late 20th century: 2052 to 2776 kg m^2 a^{-1} from 1981-87 to 2001-

07, and 1750 to 2710 kg m^2 a^{-1} from 1960-69 to 2000-08, respectively (*Potocki et al.*, 2011; *Goodwin*, 2013). Models of precipitation input for the region (*Saha et al.*, 2010; *Dee et al.*, 2011; *Lenaerts et al.*, 2012) also show a strong overall increase for the most recent decades, but some indicate a slight decline in the last decade, covering our dH/dt measurement period (*Saha et al.*, 2010; *Lenaerts et al.*, 2012; *Shepherd et al.*, 2012). The large increase and later reduction in accumulation are associated with multi-decadal warming (*Barrand et al.*, 2013) and associated reductions in sea ice extent northwest of the nAP (*Stammerjohn et al.*, 2012) recently moderated by a slight cooling trend (*Blunden and Arndt*, 2012; *Zagorodnov et al.*, 2012).

Multi-decadal accumulation, temperature and snowmelt trends cause changes in the compaction rate of snow and firn, and can potentially impact measurements of surface elevation change (*Ligtenberg et al.*, 2011). Using a model climate time series (based on reanalysis of weather data) spanning the period of our measurements (RACMO-2.1/ANT; *Lenaerts et al.*, 2012), a dH/dt for the firn column at 27 km spatial scale is obtained similar to that used in previous related analyses (*Pritchard et al.*, 2012; *Gardner et al.*, 2013). The modelled inter-annual variability in accumulation, temperature and snowmelt, and their effect on firn compaction result in dH/dt corrections between -0.19 to +0.12 m a^{-1} on the grounded ice of the nAP, with generally positive (thickening) corrections on the western side and negative to the east. The small effect on the firn layer, and the high variability of accumulation both inter-annually and among the basin areas (Figure 4a) make the correction relatively insignificant. We therefore report dH/dt as observed from the satellite data. From these observations, we report mass change in Table 1 and Table S2 as:

$$(dH/dt)_{hyps} * (A) * \rho \qquad (2)$$

where $(dH/dt)_{hyps}$ is the elevation-band-weighted mean measured dH/dt, A is area of the glacier basin or island, and ρ is our assumed mean density of ice and firn lost by dynamics (900 kg m^{-3}). We eliminated the nunatak areas from each of the basins,

based on the Antarctic Digital Database mapping of rock outcroppings in the region similar to previous studies (e.g., *Gardner et al.*, 2013).

Our estimate of mass balance for the combined nAP region is -24.9±7.8 Gt a^{-1}, with the great majority of the mass loss occurring at elevations below 1000 m a.s.l. (-21.9±6.3 Gt a^{-1}, or 88%; Table 1). Regionally, the eastern nAP basins dominate the mass loss at -17.7±3.7 Gt a^{-1}, or 72% of the loss, and of this, -15.2±3.2 Gt a^{-1} (60%) is from 12 glacier basins flowing into embayments formerly occupied by the Prince Gustav, Larsen Inlet, Larsen A, and Larsen B ice shelves. For the 11 western nAP glacier basins and islands, the mass loss rate is similar at low and high elevations (-2.3±0.7 Gt a^{-1} >1000 m a.s.l., and -2.2±1.0 Gt a^{-1} below). Overall, the nAP region accounts for ~29% of Antarctica mass imbalance during the study period (*Shepherd et al.*, 2012).

We also examined the mass balance ratio of the basins and regional areas, based on mass input, primarily snow accumulation (*Lenaerts et al.*, 2012; Table 2, Table S3). Surface mass balance (SMB) in the region has a very large gradient from west to east, with values of 1500 to 3000 kg m^{-2} a^{-1} for the western areas and high elevations dropping to ~500 to 1500 kg m^{-2} a^{-1} in the low elevation areas of the eastern nAP coast. A ratio of the mass balance divided by the mass accumulation input indicates the degree of imbalance in the glacier systems, and suggests the level of ice flux increase for glacier systems having recently accelerated due to ice front or ice shelf losses. We term this value the imbalance ratio. The imbalance ratio for the nAP as a whole is -0.45, implying that mass outflow is 45% greater during the study period relative to a steady-state rate in the current climate. For the eastern nAP glaciers, the ratio is -0.3 to -3.2 (average, -0.8) with the major ISL glaciers in the Larsen A and Larsen B between -0.33 and -3.4. The upper areas of these glacier systems are essentially balanced (~-0.1). IFL glaciers along the western and northern coastlines have imbalance ratios similar to the ISL glaciers, ~-0.5 to -2.4.

Our mass balance estimate for the nAP region agrees well with recently published

gravimetric values, although in some cases we believe this is coincidental. Recent GRACE-based estimates that can be most easily compared with our study yield values of -27.5±10 Gt a^{-1} (summing the mascons encompassing and adjacent to our study area) (*Luthcke et al.*, 2013), and 26±3 Gt a^{-1} for a larger GRACE mascon extending to 70°S (*Sasgen et al.*, 2013). Due to the low spatial resolution of the gravimetric measurement, both these GRACE-derived results inherently include portions of the Larsen C Ice Shelf and adjacent ice-covered islands we did not measure (notably, King George Island) that lost elevation and mass during the ICESat period (*Gardner et al.*, 2013). Similarly, the strong east-west gradient revealed in our study is not discernable by the GRACE system. Overall, however, the GRACE results provide a good summary confirmation for our study, and imply that nearly all of the mass loss for the Peninsula lies in, the nAP region defined here.

For earlier ICESat-only studies of the mass balance in the area (*Shepherd et al.*, 2012), the apparent agreement is likely fortuitous. Simple extrapolation methods that do not include information about individual basin dynamics (e.g., spatial/elevation extent, ice shelf loss, east-west variations), lead to very different values for total mass change. We conducted two experiments using our cross-track adjusted ICESat data alone to examine the scale of possible discrepancies. With an assumption of uniform mean elevation change for each elevation band throughout the nAP, the volume change from ICESat data would be -36.6 km^3 a^{-1}. This overestimate derives from ISL glaciers forming too great a part of the net elevation change measurement data, especially for their lower elevations. This is, in part, due to more ICESat data being acquired along the eastern nAP, likely a result of less cloud cover there. If one partially addresses this by separating ICESat data in two subsets (ISL basins vs the rest), the volume change is still 10% greater than our study, -30.6 km^3 a^{-1}.

The most recent assessment of the mass balance of the entire Peninsula uses CryoSat-2 interferometric radar altimetry data to infer a mass balance of -23±18 Gt a^{-1} for a period following our evaluation, 2010-2013 (McMillan et al., 2014). The

agreement is well within both studies' error bars, and suggests that mass imbalance for the Peninsula is not changing significantly at the present time. However, a more detailed study of a set of glacier outlets that formerly fed the Larsen A and Prince Gustav ice shelves suggests that this area (which was the site of major ice shelf disintegrations in 1988 and 1995) has begun to see a slightly reduced level of ice mass loss in the 2011-2013 period (H. Rott, pers. comm., 2014).

We now examine the potential impact of further ice shelf loss in the Scar Inlet region, a remnant ice shelf section from the Larsen B Ice Shelf. Comparing high-resolution bathymetric mapping of the seabed exposed by nAP-wide ice shelf loss and glacier retreat with our data in Figure 1 shows that it is the glaciers with deep (>500 m) troughs and recent ice shelf loss that have the greatest elevation loss and mass imbalance (*Zgur et al.*, 2007; *Shuman et al.*, 2011; *Rebesco et al.,* 2014). Recent ice-thickness maps of the tributary glaciers (Starbuck, Flask, and Leppard glaciers) of the still-intact Scar Inlet Ice Shelf (SIIS) indicate they have unusually deep glacier troughs just behind the grounding line, well in excess of 1000 m below sea level in the case of Flask Glacier, and 500 m below sea level for Starbuck glacier (*Farinotti et al.*, 2013*, Farinotti et al.,* 2014). From Table S3, the mean imbalance ratio of ISL glaciers with ice-front bathymetric troughs exceeding 500 m depth is -1.20, and -3.18 for those exceeding 1000 m depth. (for comparison, it is +0.07 for trough areas less that 500 m depth). If we assume that the three primary tributary glaciers of SIIS will experience the same mean imbalance ratio following a collapse of their frontal ice shelf in Scar Inlet, we can anticipate increased mass imbalance in those basins, from the -1.36 Gt a^{-1} observed during our study period to ~-5.5 Gt a^{-1}.

5 Conclusions

Overall, our study suggests that the nAP mass imbalance pattern is a combination of several recent changes to the coastal glaciers and ice shelf systems, likely beginning several decades ago along the western coastal fjords and islands, with extensive inland propagation of mass loss to the ice divide area, and more recent ice shelf loss along the eastern flanks and islands with extensive and expanding inland

propagation. Further, the large measured increase in snow accumulation over the past few decades has not created vast regions of positive mass balance suggesting that negative mass balances will continue into the future.

Authorship contributions

T. Scambos led the writing and compilation of graphics and tables, and with T. Haran and J. Bohlander, conducted the ICESat-based elevation change analysis. E. Berthier conducted the differential DEM analysis and integrated the ICESat data with the dDEM data. C. Shuman and A. Cook evaluated glacier front area changes and C. Shuman produced components of Figure 4. A. Cook provided the glacier basin outlines. S. Ligtenberg evaluated the firn compaction and accumulation variability estimates, and their impact on our results. All co-authors contributed to the writing of the paper.

Acknowledgements

The ICESat data for this paper are available at the NASA Distributed Active Archive Center at NSIDC (GLA12 - GLAS/ICESat L2 Antarctic and Greenland Ice Sheet Altimetry Data). The SPOT5 HRS data were provided at no cost by CNES through the SPIRIT project. The ASTER data were provided at no cost by NASA/USGS through the Global Land Ice Measurements from Space (GLIMS) project. This work was supported by NASA grant NNX10AR76G to T. Scambos and W. Abdalati, the TOSCA and ISIS programs of the French Space Agency (CNES) to E. Berthier, NASA Cryospheric Program funds to C. Shuman, NSF grant ANT-0732921 to T. Scambos, and the Netherlands Polar Program and European Union Seventh Framework Programme grant 226375 to S. Ligtenberg.

References

Barrand, N. E., Vaughan, D. G., Steiner, N., Tedesco, M., Kuipers Munneke, P., van den Broeke, M. J., and Hosking, J. S.: Trends in Antarctic Peninsula surface melting conditions from observations and regional climate modeling, J. Geophys Res., 118(1), 315–330, doi:10.1029/2012JF002559, 2013.

435 Berthier, E., Scambos, T. A., and Shuman, C. A.: Mass loss of Larsen B tributary
436 glaciers (Antarctic Peninsula) unabated since 2002, Geophys. Res. Lett., 39
437 L13501, doi:10.1029/2012GL051755, 2012.

438 Blunden, J., and Arndt, D. S.: State of the Climate in 2011, Bull. Amer. Meteor. Soc.,
439 93(7), S1–S282, doi:10.1175/2012BAMSStateoftheClimate.1., 2012.

440 Christ, A., Talia-Murray, M., Elking, N., Domack, E., Leventer, A., Lavoie, C., Brachfield,
441 S., Yoo, K.-C., Gilbert, R., Jeong, S.-M., Petrushak, S., Wellner, J.: Late Holocene
442 glacial advance and ice shelf growth in Barilari 1Bay, Graham Land, west
443 Antarctic Peninsula, Geol. Soc. Am. Bull., doi:10.1130/B31035, 2014.

444 Cook, A. J., and Vaughan, D. G.: Overview of areal changes of the ice shelves on the
445 Antarctic Peninsula over the past 50 years, The Cryosphere, 4(1), 77–98,
446 doi:10.5194/tc-4-77-2010, 2010.

447 Cook, A. J., Fox, A. J., Vaughan, D. G., and Ferrigno, J. G.: Retreating glacier fronts on
448 the Antarctic Peninsula over the past half-century, Science, 308(5721), 541–
449 544, 2005.

450 Cook, A. J., Murray, T., Luckman, A., Vaughan, D. G., and Barrand, N. E.: A new 100-m
451 Digital Elevation Model of the Antarctic Peninsula derived from ASTER
452 Global DEM: methods and accuracy assessment, Earth System Science Data,
453 *4*, 129–142, doi:10.5194/essd-4-129-2012, 2012.

454 Dee, D. P., Uppala, S. M., Simmons, A. J., Berrisford, P., Poli, P., Kobayashi, S., Andrae,
455 U., Balmaseda, M. A., Balsamo, G., Bauer, P., Bechtold, P., Beljaars, A. C. M., van
456 de Berg, L., Bidlot, J., Bormann, N., Delsol, C., Dragani, R., Fuentes, M., Geer, A.
457 J., Haimberger, L., Healy, S. B., Hersbach, H., Hólm, E. V., Isaksen, L., Kållberg,
458 P., Köhler, M., Matricardi, M., McNally, A. P., Monge-Sanz, B. M., Morcrette, J.-J.,
459 Park, B.-K., Peubey, C., de Rosnay, P., Tavolato, C., Thépaut, J.-N. and Vitart., F.:
460 The ERA-Interim reanalysis: configuration and performance of the data
461 assimilation system, Q. Jour. Royal Met. Soc., 137(656), 553–597,
462 doi:10.1002/qj.828, 2011.

463 Domack, E., Duran, D., Leventer, A., Ishman, S., Doane, S., McCallum, S., Abblas, D.,
464 Ring, J., Gilbert, R., and Prentice, M.: Stability of the Larsen B ice shelf on the
465 Antarctic Peninsula during the Holocene epoch, Nature, 436(7051), doi:
466 10.1038/nature03908, 681-685.

467 Farinotti, D., Corr, H., and Gudmundsson, G. H.: The ice thickness distribution of
468 Flask Glacier, Antarctic Peninsula, determined by combining radio-echo
469 soundings, surface velocity data and flow modelling, Ann. Glaciol., 54(63),
470 18–24, doi:10.3189/2013AoG63A603, 2013.

471 Farinotti, D., King, E. C., Albrecht, A., Huss, M., and Gudmundsson, G. H.: The bedrock
472 topography of Starbuck Glacier, Antarctic Peninsula, as measured by radio-

echo sounding, Ann. Glaciol., 55(67), 22–28, doi:10.3189/2014AoG67A025, 2014.

Favier, L., Durand, G., Cornford, S. L., Gudmundsson, G. H., Gagliardini, O., Gillet-Chaulet, F., Zwinger, T., Payne, A. J., and Le Brocq. A. M.: Retreat of Pine Island Glacier controlled by marine ice-sheet instability, Nature Clim. Change, 4(2), 117–121, doi:10.1038/nclimate2094, 2014

Flament, T., and Rémy, F: Dynamic thinning of Antarctic glaciers from along-track repeat radar altimetry, J. Glaciol., 58(211), 830–840, doi:10.3189/2012JoG11J118, 2012.

Fujisada, H., Bailey, G. B., Kelly, G. G., Hara, S., and Abrams, M. J.: ASTER DEM performance, IEEE T. Geosci. Remote Sens., 43(12), 2707–2714, 2005

Gardelle, J., Berthier, E., Arnaud, Y., and Kääb, A.: Region-wide glacier mass balances over the Pamir-Karakoram-Himalaya during 1999–2011, The Cryosphere, 7, 1263–1286, doi:10.5194/tc-7-1263-2013, 2013.

Gardner, A. S., Moholdt, G., Cogley, J. G., Wouters, B., Arendt, A. A., Wahr, J., Berthier, E., Hock, R., Pfeffer, W. T., Kaser, G., Ligtenberg, S. R. M., Bolch, T., Sharp, M. J., Hagen, J. O., van den Broeke, M. R., and Paul, F.: A Reconciled Estimate of Glacier Contributions to Sea Level Rise: 2003 to 2009, Science, 340(6134), 852–857, doi:10.1126/science.1234532, 2013.

Goodwin, B. P.: Recent Environmental Changes on the Antarctic Peninsula as Recorded in an ice core from the Bruce Plateau. PhD diss., The Ohio State University, Columbus, OH, 247 pp., 2013.

Haran, T., Bohlander, J., Scambos, T. and Fahnestock, M.: MODIS Mosaic of Antarctica 2004 (MOA2004) Image Map. Boulder, Colorado USA: National Snow and Ice Data Center, doi:10.7265/N5ZK5DM5, 2005, updated 2014.

Haran, T., Bohlander, J., Scambos, T., Painter, T., and Fahnestock, M.: MODIS Mosaic of Antarctica 2008-2009 (MOA2009) Image Map. Boulder, Colorado USA: National Snow and Ice Data Center, doi:10.7265/N5KP8037, 2014.

Howat, I. M., Joughin, I., and Scambos, T. A.: Rapid Changes in Ice Discharge from Greenland Outlet Glaciers, Science, 315(5818), 1559–1561, 2007.

Ivins, E. R., Watkins, M. M., Yuan, D.-N., Dietrich, R., Casassa, G., and Rülke, A.: On-land ice loss and glacial isostatic adjustment at the Drake Passage: 2003–2009, J. Geophys. Res.-Earth, 116, B02403, doi:10.1029/2010JB007607, 2011.

Joughin, I., Howat, I. M., Fahnestock, M., Smith, B., Krabill, W., Alley, R. B., Stern, H., and Truffer, M.: Continued evolution of Jakobshavn Isbrae following its rapid

509 speedup, J. Geophys. Res.-Earth, 113, F04006, doi:10.1029/2008JF001023,
510 2008.

511 Korona, J., Berthier, E., Bernard, M., Rémy, F., and Thouvenot, E.:SPIRIT. SPOT 5
512 stereoscopic survey of Polar Ice: Reference Images and Topographies during
513 the fourth International Polar Year (2007-2009), ISPRS J. Photogramm., 64,
514 204–212, doi:10.1016/j.isprsjprs.2008.10.005, 2009.

515 Kunz, M., King, M. A., Mills, J. P., Miller, P. E., Fox, A. J., Vaughan, D. G., and Marsh, S.
516 H.: Multi-decadal glacier surface lowering in the Antarctic Peninsula,
517 Geophys. Res. Lett., L19502, 10.1029/2012GL052823, 2012.

518 Lenaerts, J. T. M., van den Broeke, M. R., van de Berg, W. J., van Meijgaard, E., and
519 Munneke, P. K.: A new, high-resolution surface mass balance map of
520 Antarctica (1979-2010) based on regional atmospheric climate modeling,
521 Geophys. Res. Lett., 39, L04501, 4501–4501, doi:10.1029/2011GL050713,
522 2012.

523 Ligtenberg, S. R. M., Helsen, M. M., and van den Broeke, M. R.: An improved semi-
524 empirical model for the densification of Antarctic firn, The Cryosphere, 5(4),
525 809–819, doi:10.5194/tc-5-809-2011, 2011.

526 Luthcke, S. B., Sabaka, T. J., Loomis, B. D., Arendt, A. A., McCarthy, J. J., and Camp, J.:
527 Antarctica, Greenland and Gulf of Alaska land-ice evolution from an iterated
528 GRACE global mascon solution, J. Glaciol. 59, 613–631,
529 doi:10.3189/2013JoG12J147, 2013.

530 McMillan, M., Shepherd, A., Sundal, A., Briggs, K., Muir, A., Ridout, A., Hogg, A., and
531 Wingham, D.: Increased ice losses from Antarctica detected by CryoSat-2,
532 Geophys. Res. Lett. 41, 1-7, doi:10.1002/2014GL060111, 2014.

533 Mulvaney, R., Abram, N. J., Hindmarsh, R. C., Arrowsmith, C., Fleet, L., Triest, J., ... &
534 Foord, S.: Recent Antarctic Peninsula warming relative to Holocene climate
535 and ice-shelf history, Nature 489(7414), doi:10.1038/nature11391, 141-
536 144., 2012.

537 Nick, F. M., Vieli, A., Howat, I. M., and Joughin, I.: Large-scale changes in Greenland
538 outlet glacier dynamics triggered at the terminus, Nature Geosci., 2(2), 110–
539 114, 2009.

540 Nield, G. A., Barletta, V. R., Bordoni, A., King, M. A., Whitehouse, P. L., Clarke, P. J.,
541 Domack, E., Scambos, T., and Berthier, E.: Rapid bedrock uplift in the
542 Antarctic Peninsula explained by viscoelastic response to recent ice
543 unloading, Earth and Planetary Science Letters, 397, doi:
544 10.1016/j.epsl.2014.04.019, 32-41, 2014.

545 Pfeffer, W. T.: A simple mechanism for irreversible tidewater glacier retreat, J.
546 Geophys. Res.-Earth, 112 (F3), F03S25, doi:10.1029/2006JF000590, 2007.

547 Potocki, M., Mayewski, P. A., Kurbatov, A., Handley, M., Simoes, J. C., and Jaña, R.:
548 Detailed glaciochemical records from a northern Antarctic Peninsula site-
549 Detroit Plateau. In AGU Fall Meeting Abstracts, 1, p. 1822, 2011, San
550 Francisco, 5-9 December, 2011.

551 Pritchard, H. D., and Vaughan, D. G.: Widespread acceleration of tidewater glaciers
552 on the Antarctic Peninsula, J Geophys Res-Earth, 112(F3), F03S29,
553 doi:10.1029/2006JF000597, 2007.

554 Pritchard, H. D., Arthern, R. J., Vaughan, D. G., and Edwards, L. A.:Extensive dynamic
555 thinning on the margins of the Greenland and Antarctic ice sheets, Nature,
556 461(7266), 971–975, 2009.

557 Pritchard, H. D., Ligtenberg, S. R. M., Fricker, H. A., Vaughan, D. G., van den Broeke, M.
558 R., and Padman, L.: Antarctic ice-sheet loss driven by basal melting of ice
559 shelves, Nature, 484(7395), 502–505, doi:10.1038/nature10968, 2012.

560 Rebesco, M., Domack, E., Zgur, F., Leventer, A., Lavoie, C., Brachfeld, S., Willmott, V.,
561 Halverson, G., Truffer, M., Scambos, T., Smith, J., and Pettit, E.: Boundary
562 condition of grounding lines prior to collapse, Larsen-B Ice Shelf, Antarctica.
563 Science 345(6202), doi:10.1126/science.1256697, 2014.

564 Rignot, E., Casassa, G., Gogineni, P., Krabill, W., Rivera, A., and Thomas, R.:
565 Accelerated ice discharge from the Antarctic Peninsula following the collapse
566 of Larsen B ice shelf, Geophys. Res. Lett., 31, L18401, 2004.

567 Rignot, E., Bamber, J. L., van den Broeke, M. R., Davis, C., Li, Y. H., van de Berg, J., and
568 van Meijgaard, E.: Recent Antarctic ice mass loss from radar interferometry
569 and regional climate modelling, Nat. Geosci., 1(2), 106–110,
570 doi:10.1038/ngeo102, 2008.

571 Rott, H., Müller, F., Nagler, T., and Floricioiu, D.: The imbalance of glaciers after
572 disintegration of Larsen B ice shelf, Antarctic Peninsula, The Cryosphere,
573 5(1), 125–134, doi:10.5194/tc-5-125-2011, 2011.

574 Saha, S., Moorthi, S., Wu, X., Wang, J., Nadiga, S., Tripp, P., Behringer, D., Hou, Y.-T.,
575 Chuang, H.-Y., Iredell, M., Ek, M., Meng, J., Yang,, R., Mendez, M. P., van den
576 Dool, H., Zhang, Q., Wang, W., Chen, M., Becker, E. (2013). The NCEP climate
577 forecast system version 2. Journal of Climate, 27, doi:10.1175/JCLI-D-12-
578 00823.1, 2013.

579 Sasgen, I., H. Konrad, E. R. Ivins, M. R. Van den Broeke, J. L. Bamber, Z. Martinec, and
580 V. Klemann (2013), Antarctic ice-mass balance 2003 to 2012: regional
581 reanalysis of GRACE satellite gravimetry measurements with improved

582 estimate of glacial-isostatic adjustment based on GPS uplift rates, The
583 Cryosphere, 7(5), 1499–1512, doi:10.5194/tc-7-1499-2013, 2013.

584 Scambos, T. A., Haran, T. M., Fahnestock, M. A., Painter, T. H., and Bohlander, J.:
585 MODIS-based Mosaic of Antarctica (MOA) data sets: Continent-wide surface
586 morphology and snow grain size, Remt. Sens. Envron., 111(2), 242-257,
587 2007.

588 Schutz, B. E., Zwally, H. J., Shuman, C. A., Hancock, D., and DiMarzio, J. P. : Overview of
589 the ICESat mission. Geophys. Res. Lett., 32(21), L21S01, doi:
590 10.1029/2005GL024009, 2005.

591 Shepherd, A., Ivins, E. R., A, G., V. R., Bentley, M. J., Bettadpur, S., Briggs, K., Bromwich,
592 D. H., Forsberg, R., Galin, N., Horwath, M., Jacobs, S., Joughin, I., King, M. A.,
593 Lenaerts, J. T. M., Li, J., Ligtenberg, S. R. M., Luckman, A., Luthcke, S. B.,
594 McMillan, M., Meister, R., Milne, G., Mouginot, J., Muir, A., Nicolas, J. P., Paden,
595 J., Payne, A. J., Pritchard, H., Rignot, E., Rott, H., Sørensen, L. S., Scambos, T. A.,
596 Scheuchl, B., Schrama, E. J. O., Smith, B., Sundal, A. V., J. H., van de Berg, W. J.,
597 van den Broeke, M. R., Vaughan, D. G., Velicogna, I., Wahr, J., Whitehouse P. L.,
598 Wingham, D. J., Yi, D., Young, D., and Zwally, H. J.: A Reconciled Estimate of
599 Ice-Sheet Mass Balance, Science, 338(6111), 1183–1189,
600 doi:10.1126/science.1228102, 2012.

601 Shuman, C. A., Zwally, H. J., Schutz, B. E., Brenner, A. C., DiMarzio, J. P., Suchdeo, V. P.,
602 and Fricker, H. A.: ICESat Antarctic elevation data: preliminary precision and
603 accuracy assessment, Geophys. Res. Lett. 33(7), L07501, doi:
604 10.1029/2005GL025227, 2007.

605 Shuman, C. A., Berthier, E., and Scambos, T. A.: 2001-2009 elevation and mass losses
606 in the Larsen A and B embayments, Antarctic Peninsula, J. Glaciol., 57(204),
607 737–754, doi:10.3189/002214311797409811, 2011.

608 Stammerjohn, S. E., D. G. Martinson, R. C. Smith, X. Yuan, and D. Rind, D.: Trends in
609 Antarctic annual sea ice retreat and advance and their relation to El Niño–
610 Southern Oscillation and Southern Annular Mode variability, J. Geophys. Res.
611 Oceans (1978–2012), 113(C3), C03S90, doi: 10.1029/2007JC004269, 2008.

612 van den Broeke, M.,: Strong surface melting preceded collapse of Antarctic Peninsula
613 ice shelf, Geophys. Res. Lett., 32(12), L12815, doi:10.1029/ 2005GL023247,
614 2005.

615 Zagorodnov, V., Nagornov, O., Scambos, T. A., A. Muto, A., Mosley-Thompson, E.,
616 Pettit, E. C., and Tyuflin, S.: Borehole temperatures reveal details of 20th
617 century warming at Bruce Plateau, Antarctic Peninsula, *The Cryosphere*, *6*(3),
618 675–686, doi:10.5194/tc-6-675-2012, 2012.

Zgur, F., Rebesco, M., Domack, E. W., Leventer, A., Brachfeld, S., and Willmott, V.: Geophysical survey of the thick, expanded sedimentary fill of the new-born Crane fjord (former Larsen B Ice Shelf, Antarctica), US Geol. Surv. Open File Rep 1047, 2007.

Zwally, H., Schutz, R., Hancock, D., and Dimarzio, J., GLAS/ICESat L2 Antarctic and Greenland Ice Sheet Altimetry Data (HDF5). Version 33. Boulder, Colorado USA: NASA DAAC at the National Snow and Ice Data Center, doi:10.5067/ICESAT/GLAS/DATA205, 2012.

Table 1. Summary of Mass Balance for the northern Antarctic Peninsula, 2003-2008[†]

Units: Area (km^2), Mean dM/dt (Gt a^{-1}), Number of Measurements, Mean dH/dt (m a^{-1}), Mean dV/dt (km^3 a^{-1})

	Ice-Covered	Total	Ice Front Retreat			Below 1000 m a.s.l.					Above 1000 m a.s.l.			
Region	Area	dM/dt[a]	Area[b]	dH/dt[c]	dV/dt[d,h]	Area	dDEM[e]	ICESat[f]	dH/dt[g]	dV/dt[h]	Area	ICESat[f]	dH/dt[g]	dV/dt[h]
nAP <66°S, 1-33	**34222.8**	**-24.9**	**325.6**	**-7.4**	**-1.2**	**23571.7**	**44.8**	**12476**	**-1.00**	**-23.1**	**10651.7**	**2668**	**-0.31**	**-3.4**
nAP West, 1-11	**14338.2**	**-4.7**	**7.8**	**-3.9**	**-0.0**	**9014.3**	**38.6**	**2999**	**-0.27**	**-2.4**	**5323.7**	**893**	**-0.59**	**-2.8**
nAP North, 12-14	**3688.0**	**-2.3**	**4.0**	**-3.7**	**-0.0**	**3684.3**	**8.2**	**2204**	**-0.69**	**-2.5**	**3.7**	**(0)**	**(-0.31)**	**0.0**
nAP East, 15-33	**16196.4**	**-18.0**	**313.8**	**-7.5**	**-1.2**	**10872.9**	**62.4**	**7279**	**-1.67**	**-18.2**	**5323.5**	**1775**	**-0.10**	**-0.6**
Northwest AP Coast[i]	5255.1	-1.7	- -	- -	- -	3417.9	35.1	1270	-0.27	0.9	1837.0	575	-0.50	-0.9
Western IFL Glaciers[j]	**679.4**	**-1.1**	**11.8**	**-4.6**	**-0.0**	**452.1**	**35.6**	**450**	**-2.24**	**-1.0**	**226.5**	**(0)**	**-0.84**	**-0.2**
Eastern ISL Glaciers[k]	**9251.0**	**-15.2**	**305.7**	**-7.7**	**-1.1**	**6030.9**	**70.9**	**3903**	**-2.60**	**-15.7**	**3232.6**	**941**	**-0.01**	**-0.2**
James Ross Island[l]	1800.8	-2.4	47.1	-3.3	-0.1	1380.0	58.0	417	-1.93	-2.7	420.7	215	0.02	0.0
Prince Gustav tributaries[m]	1885.0	-2.7	58.2	-3.6	-0.1	1478.4	76.6	475	-2.03	-3.0	406.7	123	0.23	0.1
Larsen A tributaries[n]	3184.4	-4.5	29.3	-2.7	-0.0	2094.8	85.5	1594	-2.32	-4.9	1089.7	329	-0.08	-0.1
Larsen B ISL tributaries[o]	4181.6	-8.0	218.2	-9.5	-1.0	2457.7	55.2	1834	-3.18	-7.8	1736.2	489	-0.13	-0.2
Scar Inlet Ice Shelf trib.[p]	3524.5	-1.4	- -	- -	- -	2089.8	46.4	1965	-0.47	-0.7	1434.7	715	-0.37	-0.5

[†]Data from ICESat and satellite stereo-image differencing. ICESat data span September 2003 – March 2008. Stereo-image DEMs span 2001 to 2010.
Abbreviations for place names: nAP, northern Antarctic Peninsula; ISL, ice shelf loss; IFL, ice front loss.
[a]Assuming mean density of 900 kg/m^3 for all dV/dt measurements. Errors for these values are 0.9 times the sum of errors for dV/dt for each row.
[b]Area determined from additional ASTER, SPOT, and Landsat images, spanning 2000-2002 to 2009-2010
[c]Rate of elevation loss measured for the first 50 m elevation band above area of grounded ice retreat.
[d]Volume loss assumes flotation was reached midway between 2001 – 2010 (period of observations).
[e]Percent area covered by differential DEM satellite stereo-image data
[f]Number of repeat-track point measurements used. If <20 ICESat dH/dt measurements are available, the regional mean ICESat dH/dt for areas > 1000 m (-0.31 m a^{-1}) or, for sub-basins, the main basin mean, is used.
[g]Hypsometric weighting for areas below 1000 m elevation.
[h]Errors on dV/dt can be determined by: ±0.3 m a^{-1} * area for regions ≤1000 m a.s.l. (dDEM and ICESat data) and ±0.15 ma^{-1} * area for regions >1000 m a.s.l. (ICESat data)
[i]Glacier basins 8 – 11
[j]Glacier basins 1a, 4a, 6a, and 12a. Used dDEM data for >1000 m a.s.l. dH/dt estimate
[k]Glacier basins 19, 21-25, 26b, 27-30, and 31a.
[l]Glacier basins 17, 18, and 19
[m]Glacier basins 19 and 21
[n]Glacier basins 22-25
[o]Glacier basins 26b, 27-30, and 31a
[p]Glacier basins 31b, 32, and 33

Table 2. Comparison of total mass balance (dM/dt), input surface mass (dM_i/dt), and resulting imbalance ratio.

Units: Area, km^2; dM/dt, Gt a^{-1}; Mean dH/dt , m a^{-1}; SMB, kg m^{-2} a^{-1}; dM_i/dt, Gt a^{-1}

	Ice-Covered	Total	Mean	Mean	Total	**Imbal.**	<1000	<1000	<1000	**<1000**	>1000	>1000	>1000	**>1000**
Region	Area	dM/dt	dH/dt	SMB	dM_i/dt	**ratio**	dH/dt	SMB	dM_i/dt	**ratio**	dH/dt	SMB	dM_i/dt	**ratio**
nAP <66°S, 1-33	34222.8	-24.9	-0.77	1543	54.2	**-0.45**	-1.00	1295	29.9	**-0.70**	-0.31	2104	23.1	**-0.18**
nAP West, 1-11	14338.2	-4.7	-0.33	2112	30.4	**-0.14**	-0.27	1964	17.7	**-0.12**	-0.59	2361	12.6	**-0.17**
nAP North, 12-14	3688.0	-2.3	-0.69	537	2.0	**-1.15**	-0.69	537	2.0	**-1.15**	(-0.31)	920	0.0	**- -**
nAP East, 15-33	16196.4	-18.0	-1.20	1268	21.8	**-0.81**	-1.75	1007	10.5	**-1.56**	-0.10	1844	9.8	**-0.06**
Northwest AP Coast[a]	5255.1	-1.7	-0.35	2012	10.6	**-0.16**	-0.27	1770	6.0	**0.13**	-0.51	2458	4.5	**-0.18**
Western IFL Glaciers[b]	**679.4**	**-1.1**	**-1.77**	**1839**	**1.2**	**-1.26**	**-2.24**	**1484**	**0.7**	**-1.29**	**-0.83**	**2546**	**0.6**	**-0.28**
Eastern ISL Glaciers[c]	**9251.0**	**-15.2**	**-1.66**	**1399**	**13.0**	**-1.15**	**-2.60**	**1143**	**6.9**	**-2.05**	**-0.07**	**1898**	**6.1**	**-0.04**
James Ross Island[d]	1800.8	-2.4	-1.44	689	1.2	**-2.09**	-1.93	653	0.9	**-2.70**	0.02	834	0.4	**0.00**
Prince Gustav trib. [e]	1885.0	-2.7	-1.54	1173	2.2	**-1.23**	-2.03	968	1.4	**-1.93**	0.21	2003	0.8	**0.10**
Larsen A tributaries[f]	3184.4	-4.5	-1.55	1624	5.2	**-0.94**	-2.32	1358	2.8	**-1.58**	-0.08	2154	2.3	**-0.03**
Larsen B ISL trib.[g]	4181.6	-8.0	-1.80	1329	5.6	**-1.42**	-3.18	1064	2.6	**-2.68**	-0.13	1713	3.0	**-0.07**
Scar Inlet Ice Shelf trib.[h]	3524.5	-1.4	-0.42	1296	4.6	**-0.30**	-0.47	787	1.6	**-0.38**	-0.37	2049	2.9	**-0.16**

[a]Glacier basins 8 – 11
[b]Glacier basins 1a, 4a, 6a, and 12a
[c]Glacier basins 19, 21-25, 26b, 27-30, and 31a
[d]Glacier basins 17, 18, and 19
[e]Glacier basins 19 and 21
[f]Glacier basins 22-25
[g]Glacier basins 26b, 27-30, and 31a
[h]Glacier basins 31b, 32, and 33

Figures

Figure 1. Location and outline of basins and sub-basins in the study area, and sites of two ice cores discussed in the text. Region names, basin numbers, and abbreviations are the same as in Table S2 and S3. Major drainage basins evaluated by the study are outlined in white, sub-basins are indicated in blue. Base image is the MODIS Mosaic of Antarctica (Scambos et al., 2007). Inset, location of the study area shown in Figure 2.

Figure 2. Elevation change rates (dH/dt) and major and minor glacier basin or islands for the northern Antarctic Peninsula study area. Cyan outlines indicate the measured study basins and islands; surrounding numbers and letters refer to Table S2 and S3 entries. Magenta outlines with lower-case labels identify sub-basins within a major basin where a separate hypsometric interpolation is used. Black contour line indicates 1000 m a.s.l. elevation. Major ice shelf retreat areas since 1980 (Cook and Vaughan, 2010) are indicated in grey-blue, with years of major collapse events and the limit of extensive grounded ice loss shown. Ice edge is from a 2009 MODIS mosaic (Haran et al., 2014).

Figure 3 a-f. Hypsometry of elevation and volume changes of western basins (panel a and b; basins 1 – 11 in Table 1), eastern basins with major ice shelf loss in the period 1986 – 2009 (panels c and d; basins 19, 21-25, and 27-30 in Table 1), and basins draining to the Scar Inlet ice shelf area (panels e and f; basins31b, 32, and 33 in Table 1). Height is binned in 50 m intervals. Note that rates of elevation change trends at the highest elevations (>2000 m a.s.l., right side of left column of panels) are based on few data and are not reliable.

Figure 4. Comparison of the study area basin extents with RACMO-2 estimated SMB in kg m^{-2} a^{-1} (panel a) and mass imbalance ratio for the basin areas separated by high and low elevation areas (above and below 1000 m; panel b).

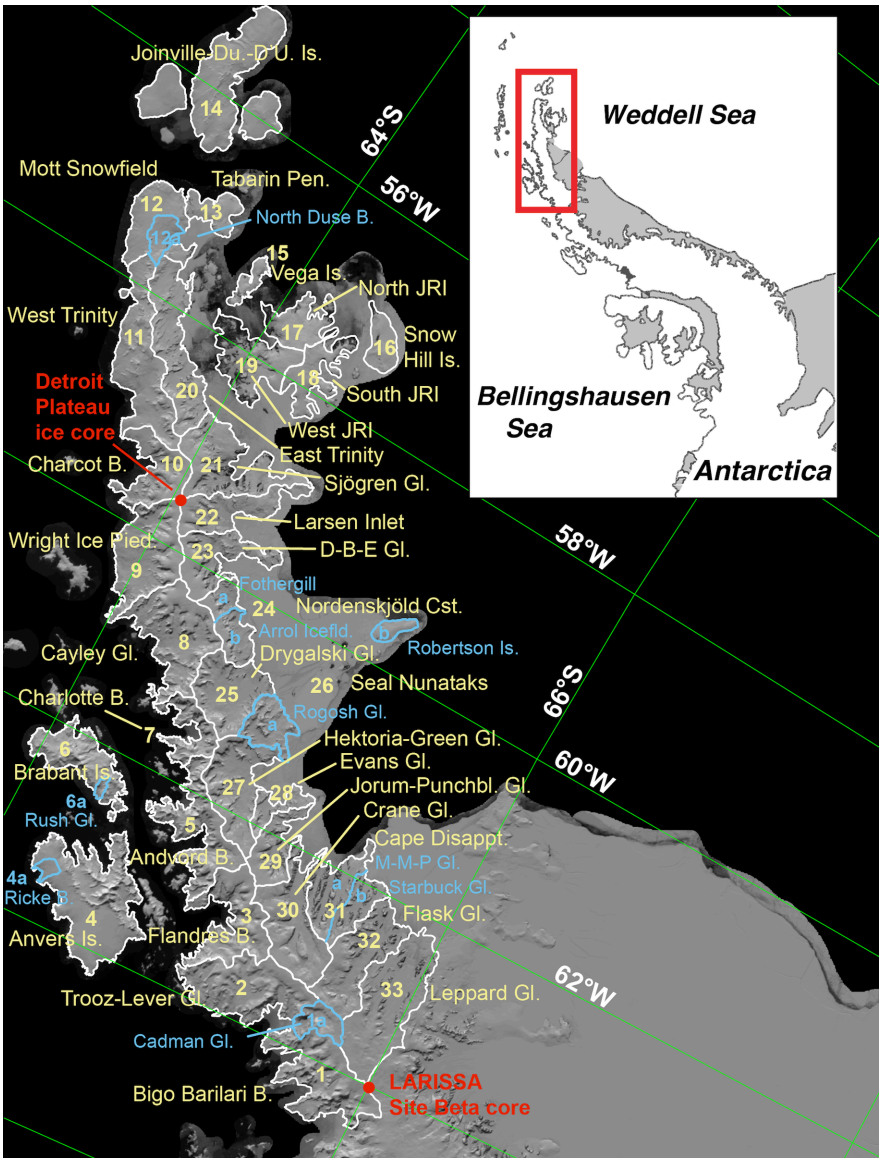

726

727 **Figure 1**. Locations and outlines of basins and sub-basins in the study area, and sites of two
728 climate ice cores discussed in the text. Region names, basin numbers, and abbreviations are
729 the same as in Tables S2 and S3. Major drainage basins are outlined in white, sub-basins are
730 indicated in blue. Base image is the MODIS Mosaic of Antarctica (MOA2004; *Scambos et al.*,
731 2007; *Haran et al.,* 2005). Inset, location of the study area shown in Figure 2.

732

733

734

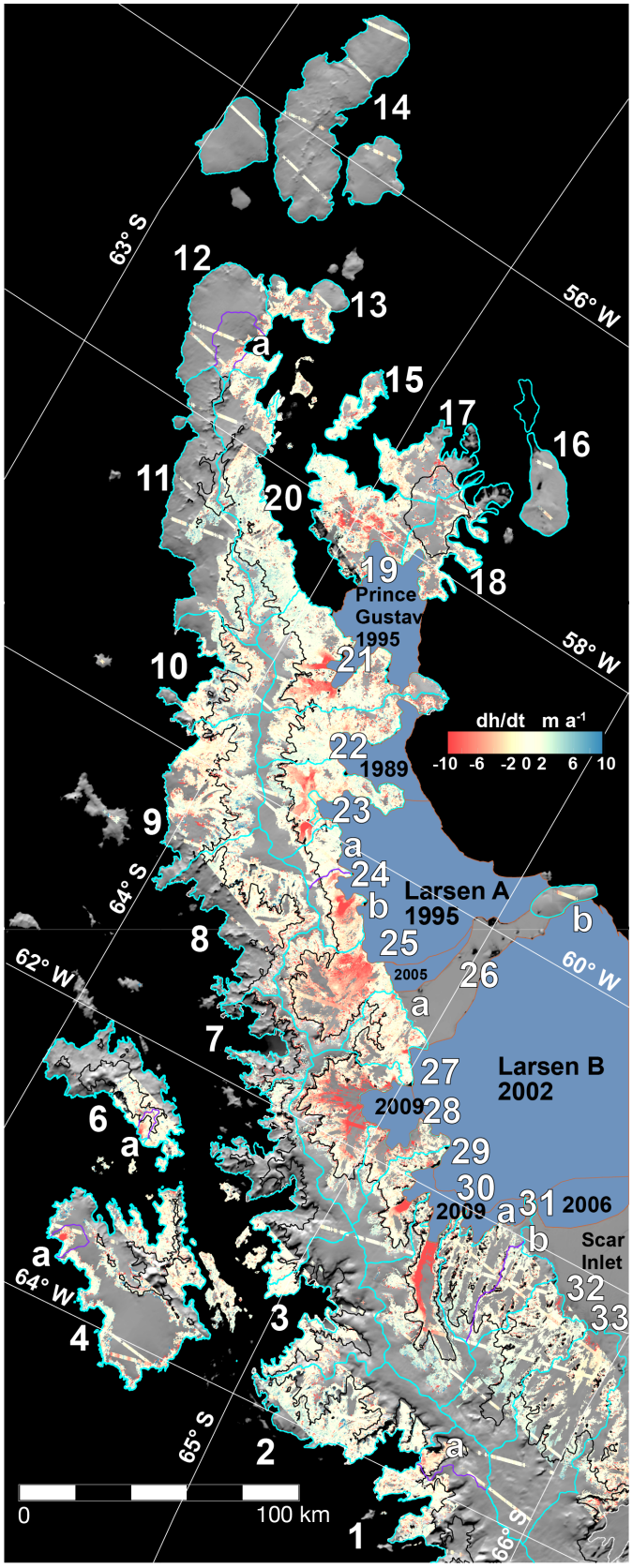

Figure 2. Elevation change rates (dH/dt) and major and minor glacier basin or islands for the northern Antarctic Peninsula study area. Cyan outlines indicate the measured study basins and islands; adjacent numbers and letters refer to Table S2 and S3 entries. Magenta outlines with lower-case labels identify sub-basins within a major basin where a separate hypsometric interpolation is used. A black line indicates the 1000 m a.s.l. elevation contour. Major ice shelf retreat areas since 1980 (*Cook and Vaughan*, 2010) are indicated in blue, with years of major collapse events and the limit of extensive grounded ice loss shown. Ice edge is from a 2009 MODIS mosaic (MOA2009; *Haran et al.,* 2014).

735

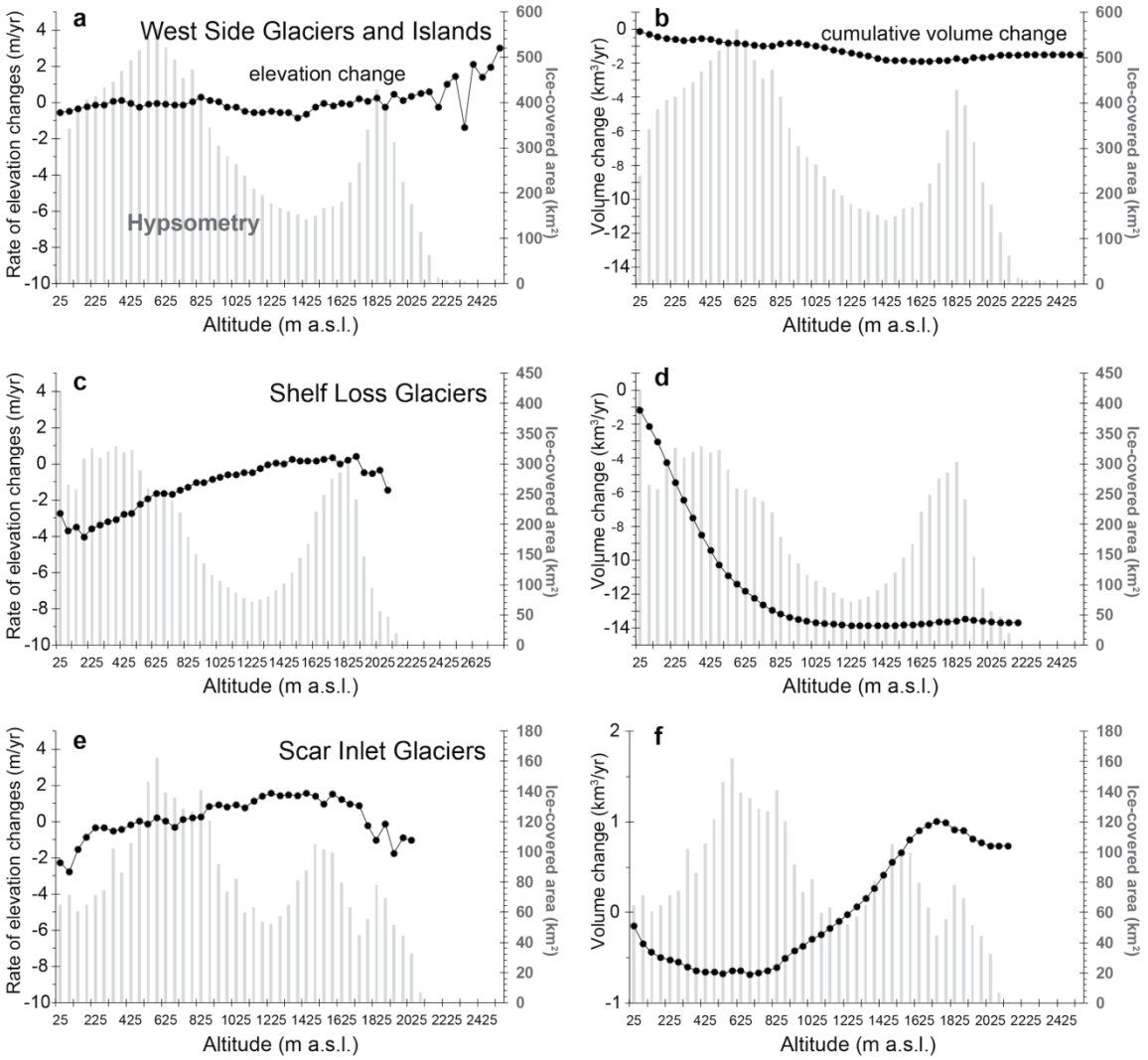

Figure 3 a-f. Hypsometry of elevation and volume changes of western nAP basins (panel a and b; basins 1 – 11 in Table S2 and S3), eastern nAP basins with major ice shelf loss in the period 1986 – 2009 (panels c and d; basins 19, 21-25, and 27-30 in Table S2 and S3), and basins draining to the Scar Inlet ice shelf area (panels e and f; basins 31b, 32, and 33 in Tables 1 and 2 and Tables S2 and S3). Height is binned in 50 m intervals. Rates of elevation change trends at the highest elevations (>2000 m a.s.l., right side of left column of panels) are based on few data and are not reliable.

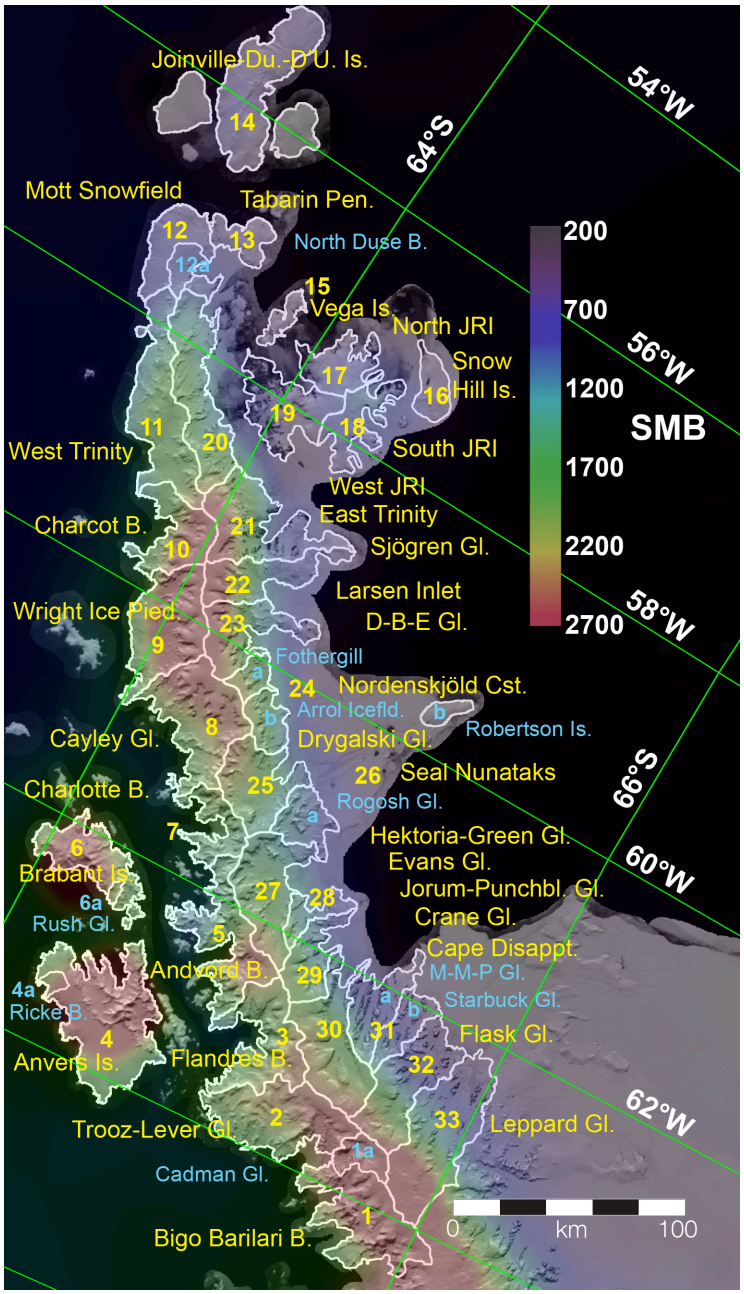

748

749 **Figure 4a.**

750 **Figure 4 a and b.** Comparison of the study area basin extents with RACMO-2

751 estimated SMB in kg m^{-2} a^{-1} (a) and mass imbalance ratio for the basin areas

752 separated by high and low elevation areas (above and below 1000 m; b).

753

754

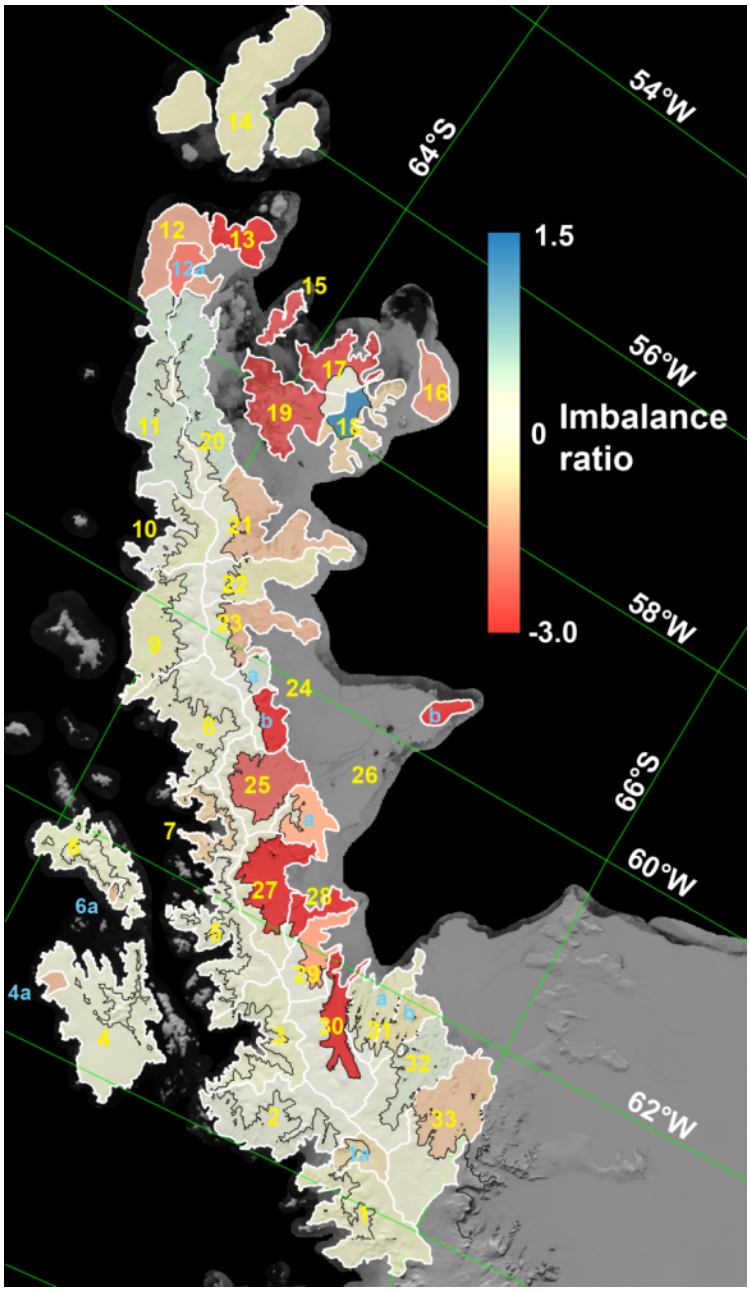

Figure 4b

Figure 4 a and b. Comparison of the study area basin extents with RACMO-2 estimated SMB in kg m^{-2} a^{-1} (a) and mass imbalance ratio for the basin areas separated by high and low elevation areas (above and below 1000 m; b).